Smart Structures and Systems, *Vol. 25, No. 5 (2020) 543-557*
DOI: https://doi.org/10.12989/sss.2020.25.5.543

Investigations on a vertical isolation system with quasi-zero stiffness property

Ying Zhou* and Peng Chen [a]

State Key Laboratory of Disaster Reduction in Civil Engineering, Tongji University, 200092 Yangpu District, Shanghai, China

(*Received July 16, 2019, Revised November 21, 2019, Accepted December 24, 2019*)

Abstract. This paper presents a series of experimental and numerical investigations on a vertical isolation system with quasi-zero stiffness (QZS) property. The isolation system comprises a linear helical spring and disk spring. The disk spring is designed to provide variable stiffness to the system. Orthogonal static tests with different design parameters are conducted to verify the mathematical and mechanical models of the isolation system. The deviations between theoretical and test results influenced by the design parameters are summarized. Then, the dynamic tests for the systems with different under-load degrees are performed, including the fast sweeping tests, harmonic excitation tests, and half-sine impact tests. The displacement transmissibility, vibration reduction rate, and free vibration response are calculated. Based on the test results, the variation of the transmission rule is evaluated and the damping magnitudes and types are identified. In addition, the relevant numerical time history responses are calculated considering the nonlinear behavior of the system. The results indicate that the QZS isolation system has a satisfactory isolation effect, while a higher damping level can potentially promote the isolation performance in the low-frequency range. It is also proved that the numerical calculation method accurately predicts the transmission character of the isolation system.

Keywords: quasi-zero stiffness; static test; dynamic test; transfer function

1. Introduction

Linear isolation technology has been widely investigated and used in engineering practices (Rivin 2003, Chopra 1995, Zhou and Chen 2017). An isolation device with linear stiffness can reduce the response vibration within the frequency range $\Omega > \sqrt{2}\omega_n$ (Ω is the excitation frequency and ω_n is the natural frequency of the isolation system). The linear isolation system is effective only when the aforementioned condition is met. However, several types of excitations such as environment vibration, impact, earthquake, wind, etc. consist of low-frequency vibration components that are harmful to the system (Sciulli and Inman 1998).

Better performance in the low-frequency range can be obtained by adding the effective mass to lower the natural frequency of the isolation system. Physical lever with additional mass (Rita *et al*. 1978), hydraulic lever (Goodwin 1965, Halwes and Simmons 1980) or inertial devices (Lu *et al*. 2017, Loh and Chao 1996, Lin *et al.* 2018) has been proposed to promote the isolation effect. These types of isolators are called the ‘anti-resonant vibration isolator’ and they also belong to the linear stiffness type isolation systems.

Instead of using linear stiffness components in the isolation system, researchers investigated the isolation systems with nonlinear stiffness behavior. There are two types of nonlinear stiffness isolation systems. The first type utilizes the geometric nonlinearity character of the system including the torsional crank linkage (Winterflood and Blair 1998), folded pendulum isolator (Blair *et al*. 1994), X-pendulum isolation table (Demetriades *et al*. 1993), conical pendulum (Winterflood *et al*. 1999), and Euler column isolator (Budiansky 1974) among others.

The other type of nonlinear stiffness isolator combines the negative stiffness device (NSD) with the positive stiffness device to obtain a lower effective natural frequency for the isolation system. Owing to the significant reduction in stiffness, several types of nonlinear stiffness isolators are also referred to as quasi-zero stiffness (QZS) isolators by some researchers. Several vibration protection systems with QZS property were first defined and documented by Alabuzhev *et al*. (1989). Platus (1992) proposed an NSD for linear vertical isolation systems based on horizontal pre-loaded hinged links. It was concluded that the natural frequency of the combined system can be designed between 1 Hz to 10 Hz. Carrella *et al.* (2009) similarly used pre-stressed horizontal helical spring to provide negative stiffness at the balanced position of a vertical isolation system. By using Taylor expansion, the controlling equation of motion can be simplified as a classic Duffing equation and the theoretical solutions are accordingly given. A novel type of NSD based on pre-stressed helical spring was designed by Sarlis *et al*. (2012), Pasala *et al*. (2014) and Chen *et al*. (2015), which can be adopted in building structures to reduce the seismic action. Cimellaro *et al*. (2018) proposed the use of pre-stressed helical spring to design a three-dimensional seismic isolator. Other negative stiffness constructions include the magnetic NSD (Shi and Zhu 2015, 2017, Zheng *et al*. 2018, Shi *et al*. 2018), rotation-based NSD (Walsh *et al*. 2018), and bio-

*Corresponding author, Professor,
E-mail: yingzhou@tongji.edu.cn
[a] Ph.D. Student, E-mail: 100751@tongji.edu.cn

http://www.techno-press.org/?journal=sss&subpage=7 ISSN: 1738-1584 (Print), 1738-1991 (Online)

inspired passive negative spring (Kwon *et al*. 2015).

Generally, the basic requirement of isolation impedes the use of vertical isolation technology owing to (1) large initial static settlement from gravity loads and (2) large isolation drift or rocking movement under low-frequency and large magnitude input (Gazi and Alhan 2018, Guzman Pujols and Ryan 2018, Farsangi *et al*. 2018, Hu *et al*. 2017). The disk spring can provide the negative stiffness and considerably large loading capacity at its flat position. Therefore, it is preferable to be used as NSD in a vertical isolation system than other NSDs. A QZS vertical isolation system that combines the helical and disk springs is proposed by Meng *et al*. (2015) and the transmissibility curves are derived theoretically. Zhou *et al*. (2019) designed a novel three-dimensional isolator with the vertical QZS and horizontal friction pendulum systems. The theoretical solutions are compared using different analytical methods and the isolation effect is checked using time history numerical analysis.

Based on the literature review, previous theoretical and numerical studies have been conducted to investigate the static and dynamic properties of the proposed vertical QZS isolation device. However, the complex static and dynamic mechanical behavior have not been fully verified by experiments. Building on previous work, the main academic contributions of this study are: (1) verifying the force-displacement relation varied with two design parameters of the proposed QZS isolation system via static tests; (2) revealing the variation law of the dynamic properties of the isolation system influenced by different under-load degrees and excitation amplitudes by comparing transmissibility curves in different dynamic test situations; (3) Identifying the damping type and the frequency-dependent damping levels of the isolation system; (4) Evaluating the isolation effect of the QZS isolation system under harmonic and impact excitations based on experiment results and corresponding numerical simulations.

2. Static compression tests

2.1 Force-displacement relation

Fig. 1 presents the cross-section sketch of a disk spring. The restoring force of a disk spring can be expressed using a third order equation as shown below (Meng *et al*. 2015).

$$F_d(x) = \frac{2\pi E x}{(d_1-d_2)^2(1-\mu^2)} \left\{ \left[\frac{1}{2}(d_1^2-d_2^2) - \frac{(d_1-d_2)^2}{ln\frac{d_1}{d_2}} \right] \left(\frac{h}{r_1-r_2} - \frac{x}{d_1-d_2} \right) \left(\frac{h}{r_1-r_2} - \frac{x}{2(d_1-d_2)} \right) t + \frac{t^3}{12} ln\frac{d_1}{d_2} \right\} \tag{1}$$

where r_1 and r_2 are the external and internal radius, d_1 and d_2 are the distance between the central axis and the under- and upper-loading positions, h is the height of the inner cone, and t is the thickness of disk spring. E and μ represent the elastic modulus and the Poisson ratio of the material, respectively. The geometric dimensions and load position of the disk spring are also illustrated in Fig. 1.

The QZS system is obtained by connecting the disk spring and helical spring in parallel. The restoring force of the system is given as

$$F_{QZS} = F_d + F_l = F_d + kx \tag{2}$$

where F_l is the restoring force of the helical spring and k is the linear stiffness.

Two design parameters with thickness ratio r and loading position ratio C are proposed for designing the disk spring and the proposed QZS isolation system.

$$r = \frac{h}{t} \tag{3}$$

$$C = \frac{d_1}{d_2} \tag{4}$$

2.2 Loading setups and specimens

The static tests were performed using the MTS809 loading system at the Engineering Mechanic Test Center of Tongji University. They are designed to verify the static and mechanic properties of the QZS system with variable design parameters r and C. The photographs of the test are shown in Fig. 2. The experiment loading rate is 0.8 mm/min.

To test the QZS system with different design parameters, replaceable specimens are designed in the QZS loading system. The schematic illustration is shown in

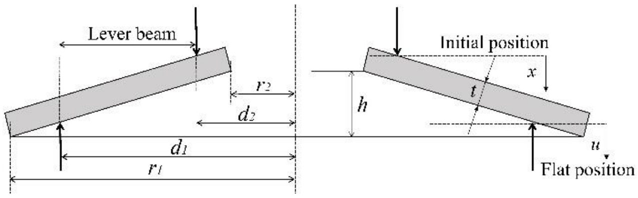

Fig. 1 Cross section schematic diagram of disk spring

(a) (b)

Fig. 2 Test photograph of (a) MTS809 loading system; and (b) QZS isolation loading system

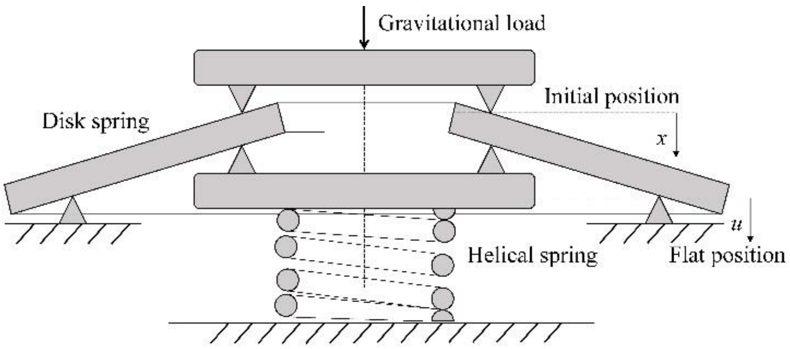

(a)

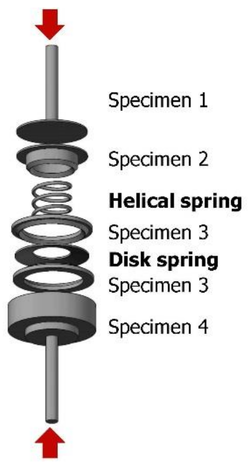

(b)

Fig. 3 Illustration of (a) QZS loading system; and (b) overall loading system assembly

Table 1 Different loading parameters

Case number	Loading distant ratio $C = d_1/d_2$	Under-loading distance d_1	Upper-loading distance d_2
No. 1	1.62	47.0 mm	29.0 mm
No. 2	1.50	45.0 mm	30.0 mm
No. 3	1.29	45.0 mm	35.0 mm

Table 2 Different size of disk springs

Case number	Thickness ratio $r = h/t$	Height of inner cone h	Thickness t
No. 1	2.41	5.3 mm	2.2 mm
No. 2	2.78	5.0 mm	1.8 mm
No. 3	3.00	4.5 mm	1.5 mm

Fig. 3. The value of effective thickness ratio r and loading position ratio C can be changed by using different types of disk spring and loading specimens (specimens 2 and 3 are manufactured to change the value of C). The helical spring is identical throughout the experiment. The specimens 1 and 4 are designed as connection parts to the loading system.

The different design values of r and C are listed in Tables 1-2. The external and internal radii of disk spring are 100.0 mm and 52.0 mm, respectively, for the three types of disk spring. The following orthogonal static tests are designed based on the combination of every two different design parameters listed in the two tables.

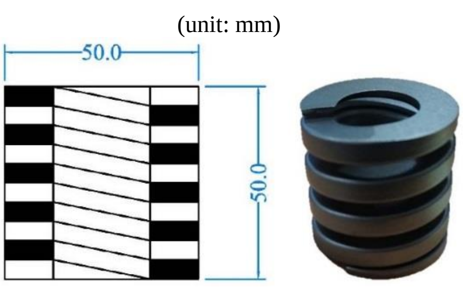

(a)

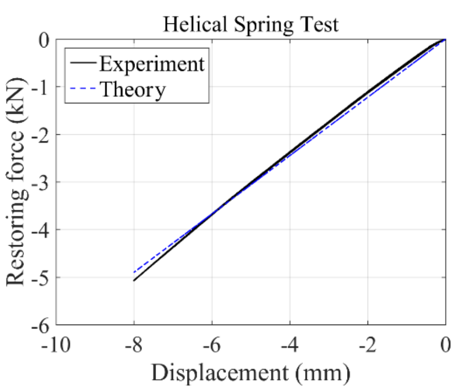

(b)

Fig. 4 Static compression experiment for helical spring (a) photograph; and (b) test results

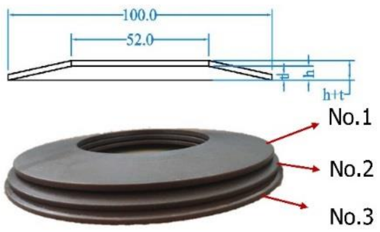

(unit: mm)

Fig. 5 Photograph of three types of disk spring

2.3 Static compression test for helical spring

The uniaxial compression experiment for the helical spring is performed to verify the mechanical properties with theoretical design values. The design stiffness for the linear helical spring is k = 0.613 kN/mm and the tested equivalent linear stiffness is k = 0.635 kN/mm. The comparison between the designed theoretical force-displacement relation and tested results are shown in Fig. 4. The helical spring shows an ideal linear behavior that accurately correlates with the design value.

2.4 Static compression test for disk spring

Three different types of disk spring are shown in Fig. 5. The first disk spring and loading case are selected. The test results for a single disk spring and two stacked springs are shown in Fig. 6. It is concluded that the restoring force of the disk spring is smaller than the theoretical results but the consistency of the stiffness curves is better than that of the

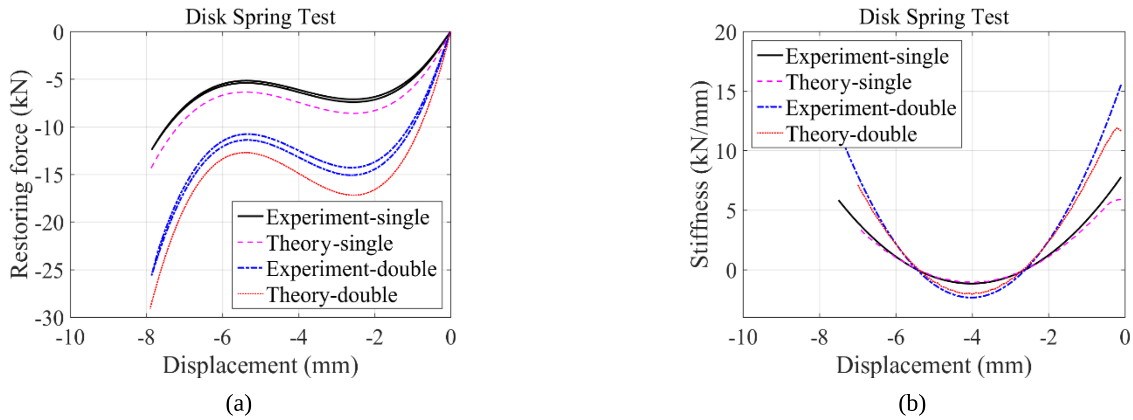

Fig. 6 Static compression experiment for helical spring (a) photograph; and (b) test results

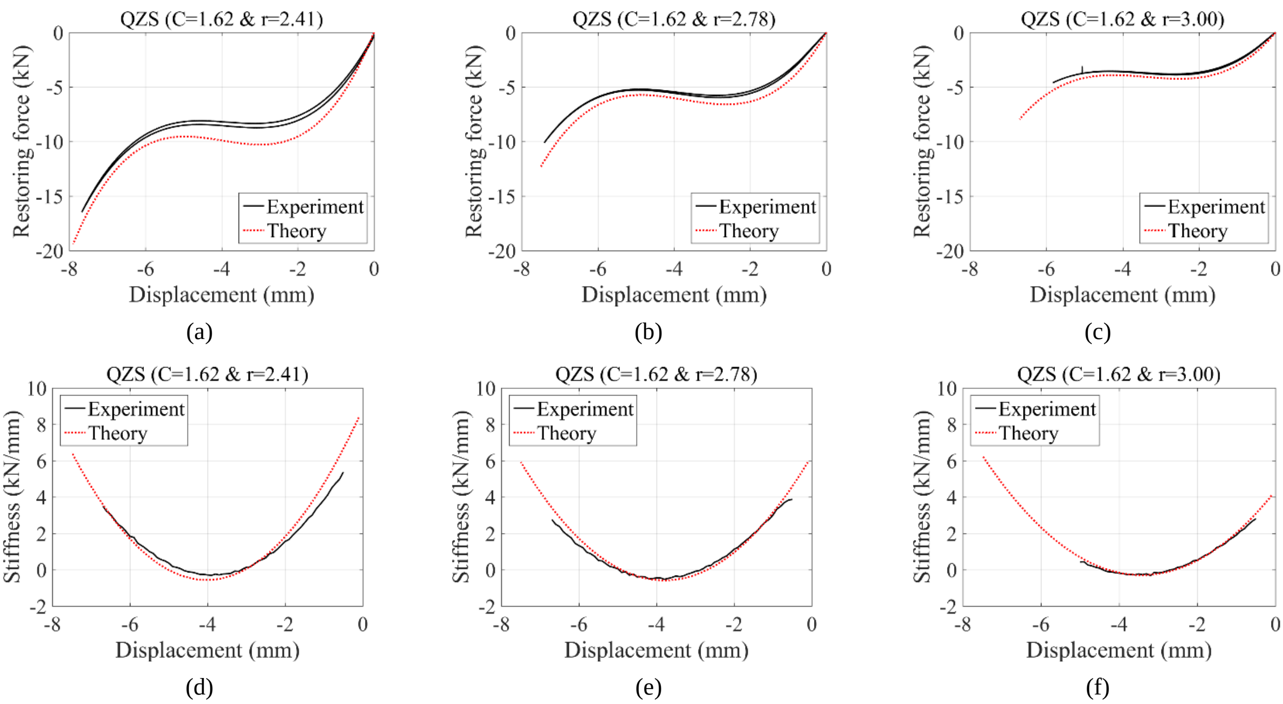

Fig. 7 Static compression experiment for QZS isolation system of (a) restoring force of test No. 1; (b) restoring force of test No. 2; (c) restoring force of test No. 3; (d) stiffness of test No. 1; (e) stiffness of test No. 2; and (f) stiffness of test No. 3

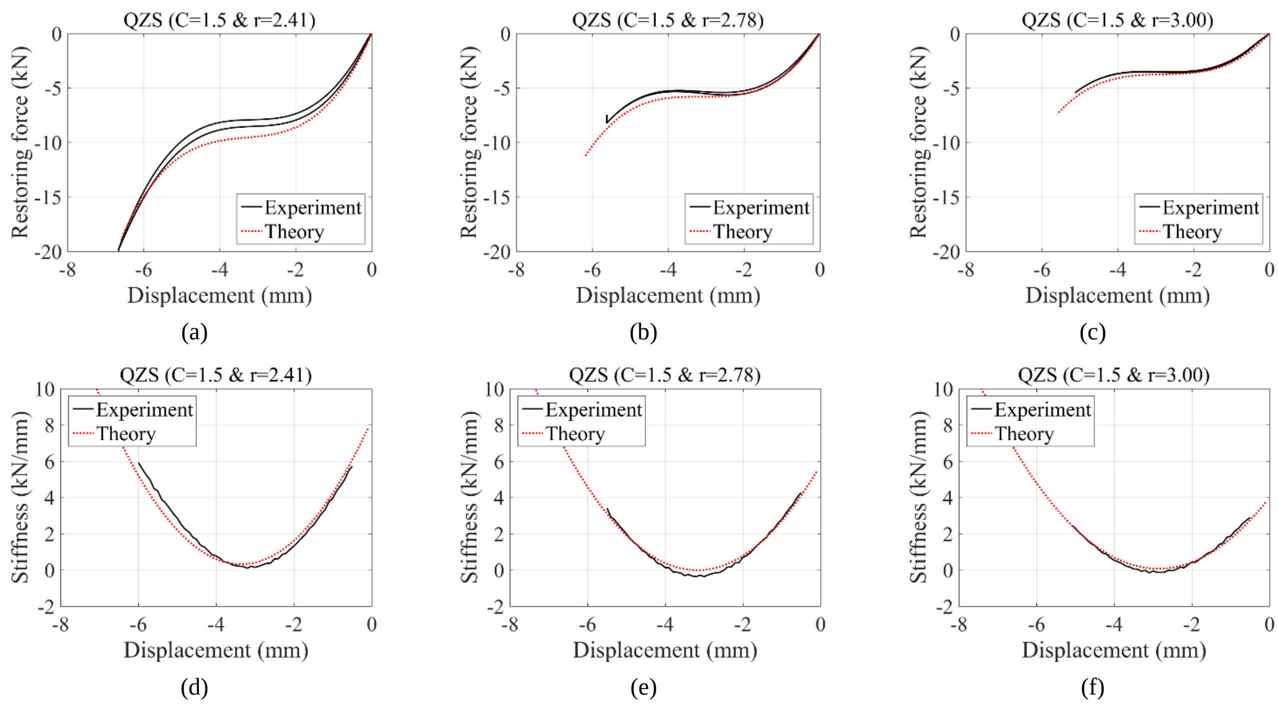

Fig. 8 Static compression experiment for QZS isolation system of (a) restoring force of test No. 4; (b) restoring force of test No. 5; (c) restoring force of test No. 6; (d) stiffness of test No. 4; (e) stiffness of test No. 5; and (f) stiffness of test No. 6

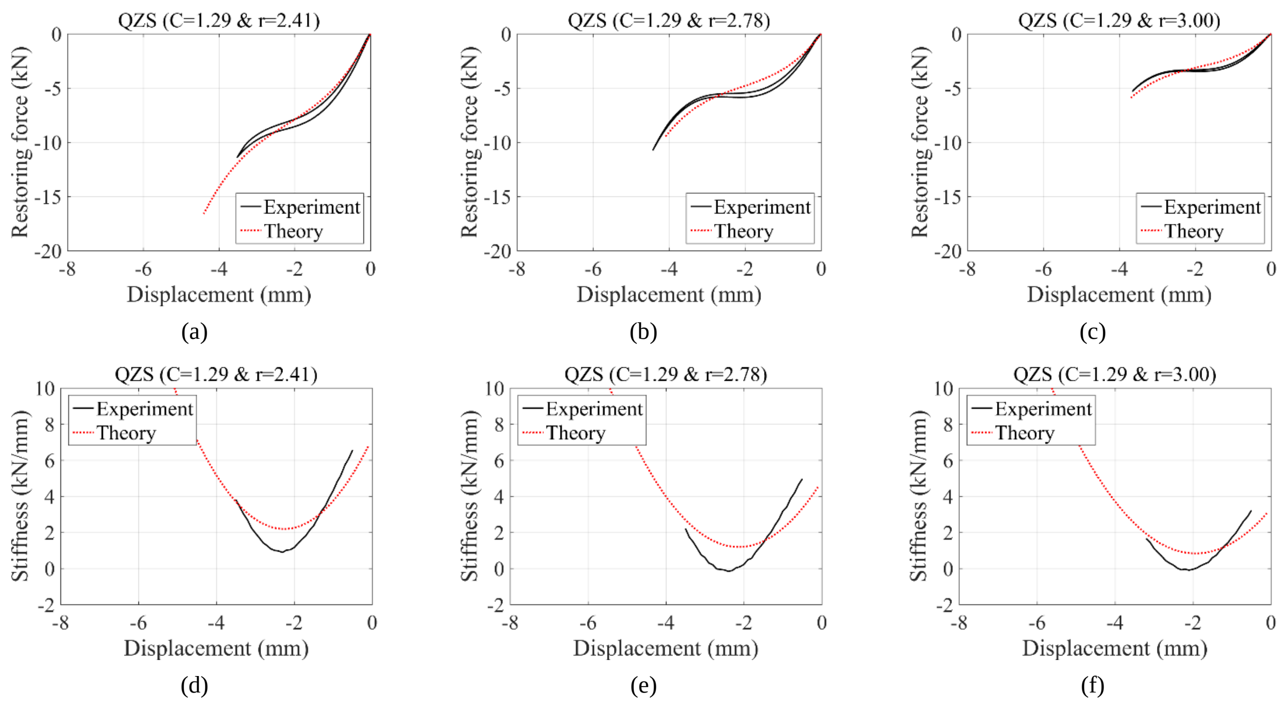

Fig. 9 Static compression experiment for QZS isolation system of (a) restoring force of test No. 7; (b) restoring force of test No. 8; (c) restoring force of test No. 9; (d) stiffness of test No. 7; (e) stiffness of test No. 8; and (f) stiffness of test No. 9

force curves. For the stacked springs, the mechanical properties are the product of mechanical properties of one spring multiplied with the number of springs.

2.5 Static compression test for QZS system

Orthogonal static loading tests for different sizes of disk spring and loading parameters listed in Tables 1-2 are conducted. The comparison between the test results and

Table 3 List of orthogonal static test

	C = 1.62	C = 1.50	C = 1.29
r = 2.41	No. 1	No. 4	No. 7
r = 2.78	No. 2	No. 5	No. 8
r = 3.00	No. 3	No. 6	No. 9

theoretical curves are presented in Figs. 7-9. The test cases and their corresponding test number are listed in Table 3.

To evaluate the deviations between the theoretical predictions shown in Eq. (1) and experiment results, the root mean squared error (RMSE) is defined as

$$\text{RMSE}=\sqrt{\frac{1}{n}\sum_{i=1}^{n}(x_i-\bar{x}_i)^2} \tag{5}$$

where n is the number of data points, x_i is the tested value, and $\bar{x}_i$ is the corresponding theoretical value.

Fig. 10 compares the RMSE for the restoring force and stiffness of different QZS isolation systems. The results indicate that the force and stiffness deviations for the test cases with C = 1.29 and 1.62 are significantly larger than in other cases. It is concluded that the loading position ratio C influences the applicability of the theory equations and an appropriate value of C is important for designing a QZS isolation system. The variation of the disk spring thickness ratio r does not have a remarkable influence on the deviations. Another two important mechanical properties of the QZS isolation system are the flat loading force and flat stiffness, which can decide the vertical loading capacity and isolation effect of the system. The experiment results for different cases are compared with the theoretical results in Fig. 11. The results of the experiment forces are closer to the theoretical value, while the relative error of the flat stiffness is larger. The test results indicate that for designing a QZS system, enough stiffness margin should be kept avoiding negative stiffness.

3. Shake table experiment

3.1 Loading setups and specimens

Shake table experiments are conducted to verify the dynamic properties, design theories, and isolation effect of the QZS isolation system. The dynamic experiment was performed at the State Key Laboratory of Disaster Reduction in Civil Engineering, Tongji University. DC-20000 electromagnetic shake table is used to impose

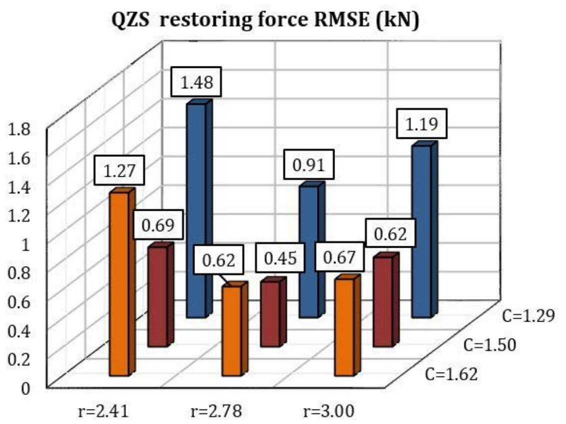

(a)

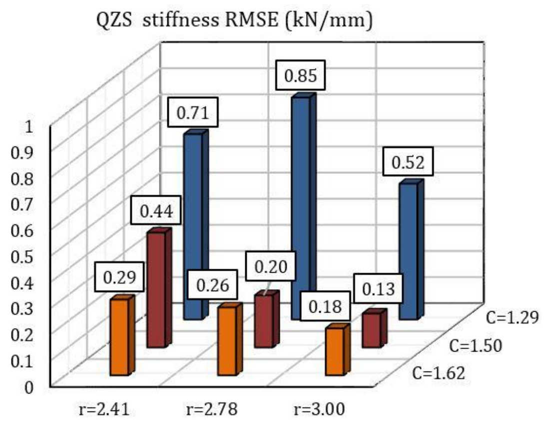

(b)

Fig. 10 RMSE for different QZS isolation system of (a) restoring force; and (b) stiffness

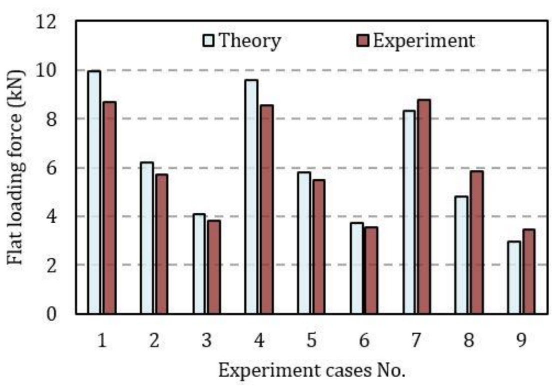

(a)

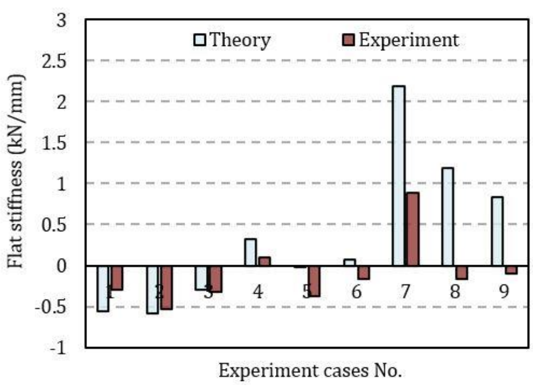

(b)

Fig. 11 The comparison between test and theoretical results on (a) flat loading force; and (b) flat stiffness

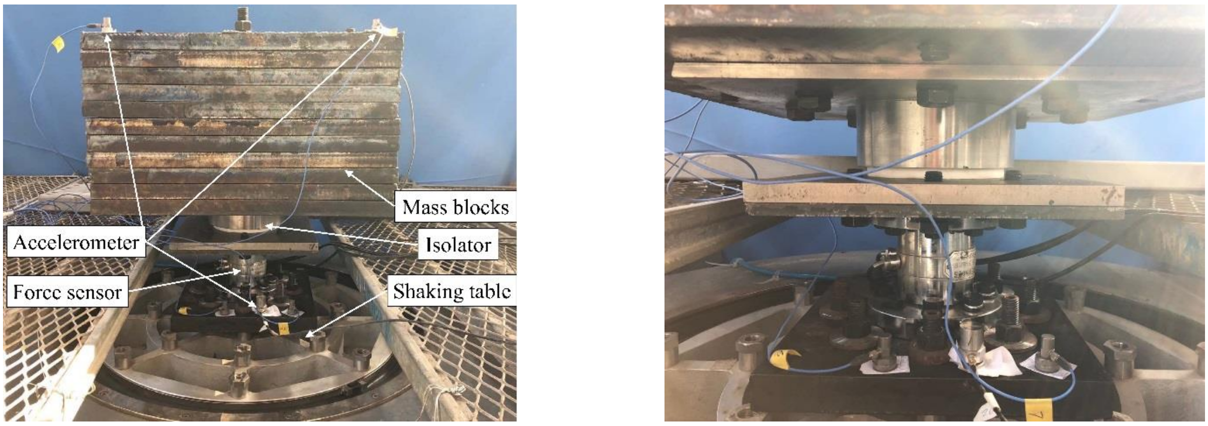

(a) (b)

Fig. 12 Photograph of (a) overall test system; and (b) QZS isolation system and force sensor

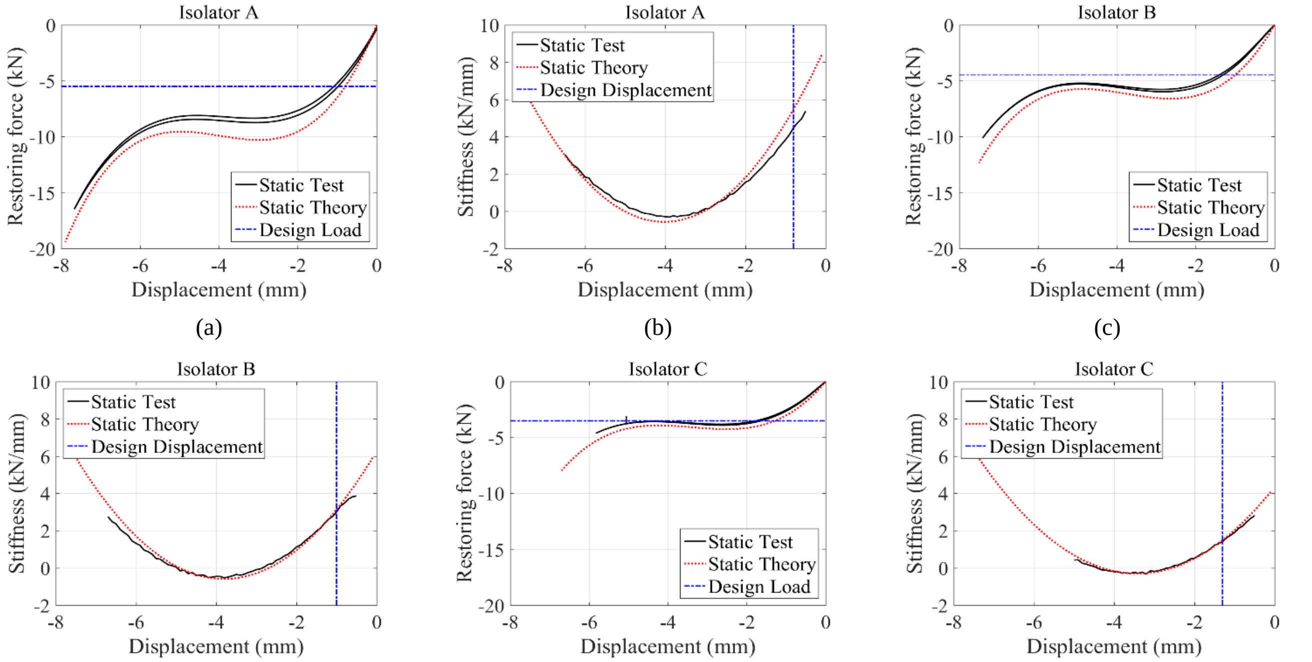

(a) (b) (c) (d) (e) (f)

Fig. 13 Static mechanic properties and design upper-load of (a) restoring force of isolator A; (b) stiffness of isolator A; (c) restoring force of isolator B; (d) stiffness of isolator B; (e) restoring force of isolator C; and (f) stiffness of isolator C

vertical vibrations on the isolation systems. The experiment photographs are shown in Fig. 12. Different numbers of the mass blocks are used to meet the upper-load requirement. The accelerometers are placed on the top of mass blocks and shaking table to record the time history acceleration response, and the force sensor is set to ensure the accuracy of the upper-load.

Three different QZS isolation systems are tested in accordance with the static tests with C = 1.50 and r = 2.41, 2.78, and 3.00. The three systems have the same value of C but different values of r, and they are numbered as isolator A (r = 2.41), isolator B (r = 2.78) and isolator C (r = 3.00). To reflect the real situations of vertical QZS isolation in engineering, the experiment system is designed to be loaded in the under-load states instead of fully loaded at the flat position of disk springs. The under load state is designed in the experiment considering the QZS force range is narrow. The under load state can reflect the real engineering application situation with the variable upper payload. To broaden the QZS force range and increase the displacement capability of the system, two or more disk springs can be connected in series in the vertical direction, so that the isolation performance of the system can be potentially promoted.

The degree of under-load decreases from isolator A to isolator C, static and mechanical properties and the design load for different isolators are shown in Fig. 13. The upper-loading mass for isolator A-C is 550, 450, and 350 kg, respectively.

3.2 Frequency sweeping test

Frequency sweeping tests are conducted for the three types of isolators to verify the change rule in dynamic properties of the QZS system with different input magnitudes and degrees of under-load considering the input displacement and acceleration control. The input frequency increases at a logarithmic speed of 30 s for each 1/3rd octave. The detail descriptions of frequency sweeping tests are listed in Table 4.

Transfer functions are calculated to evaluate the dynamic properties of the systems. The Levy method is used to obtain the fitted curves based on raw data. Typical raw transfer functions and fitted curves are shown in Fig. 14 (the fitted curves can accurately describe the ragged raw data and the following discussions are generally based on the fitted results).

The equivalent natural frequencies and linear viscous damping ratios are calculated and listed in Table 5. The variation in absolute values of the transfer functions are shown in Fig. 15. The change rule of the natural frequency under different input amplitudes is remarkable because the natural frequency declines with the decrease in under-load degree and increase in input magnitude.

The first rule states that when the static balance position is close to the flat position of disk spring, smaller tangent stiffness is obtained, as depicted in Fig. 13. For the frequency change rule under different input magnitudes, the principles can be explained using displacement-dependent equivalent stiffness. For the under-load point of the QZS system, a larger response displacement corresponds to a smaller equivalent secant stiffness. As illustrated in Fig. 16, the equivalent stiffness K_{eq1} is larger than K_{eq2}. However, for the full-load point of the system, the change rules are on the opposite. The change rules of the damping properties are not significant under the frequency sweeping test. They are discussed in the following sections.

Table 4 List of frequency sweeping test

Isolator type	Test number	Control type	Input magnitude	Frequency range
Isolator A	SP1	displacement	0.125 mm	5-35.5 Hz
	SP2	displacement	0.250 mm	5-35.5 Hz
	SP3	displacement	0.500 mm	5-35.5 Hz
	SP4	acceleration	1 m/s2	5-120 Hz
Isolator B	SP5	displacement	0.125 mm	5-35.5 Hz
	SP6	displacement	0.250 mm	5-35.5 Hz
	SP7	displacement	0.500 mm	5-35.5 Hz
Isolator C	SP8	displacement	0.125 mm	5-35.5 Hz
	SP9	displacement	0.250 mm	5-35.5 Hz
	SP10	displacement	0.500 mm	5-35.5 Hz

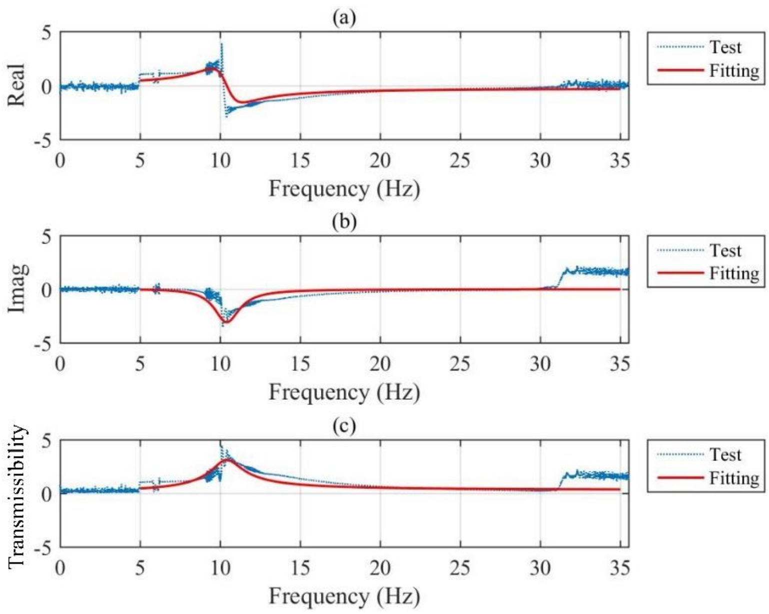

Fig. 14 Typical transfer function of frequency sweeping test (SP3), (a) real part of the transimissibility; (b) imaginary part of the transmissibility, and (c) absolute value of the transimissibility

Table 5 Test results of equivalent natural frequency and viscous damping ratio

	SP1	SP2	SP3	SP4	SP5	SP6	SP7	SP8	SP9	SP10
Frequency (Hz)	15.62	13.67	10.42	23.81	11.67	11.15	9.53	10.89	10.20	9.03
Damping ratio (%)	16.38	9.71	9.24	24.78	6.09	7.70	11.15	6.16	7.67	7.02

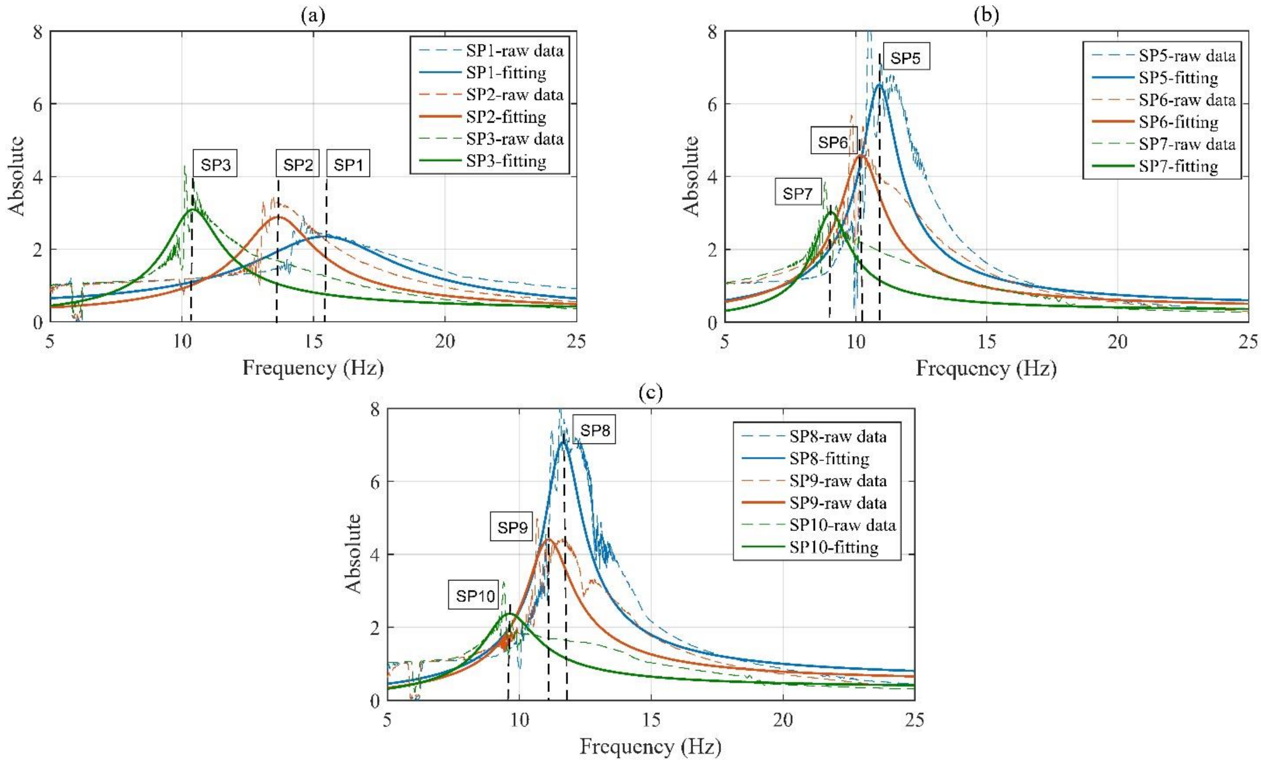

Fig. 15 Absolute value of transfer function of (a) isolator A; (b) isolator B; and (c) isolator C

3.3 Harmonic vibration tests

The harmonic vibration tests with the same input displacement amplitude and different frequencies are conducted. The results are compared to test the acceleration and displacement transmission properties of the QZS system. Based on the response of the QZS isolation system and input vibration at the shake table, the acceleration reduction (AR) ratio (corresponding to the absolute transmissibility) and relative displacement amplification (DA) ratio (corresponding to the relative transmissibility) are defined and calculated as

$$\mathrm{AR} = \frac{A_r}{A_i} \tag{6}$$

$$\mathrm{DA} = \frac{D_r}{D_i} \tag{7}$$

where A_r is the absolute acceleration response amplitude of the QZS system and A_i is the input acceleration amplitude. D_r is the relative displacement amplitude of the system and D_i is the input displacement amplitude. It should be noted that all data is obtained in the stable response phase of the isolation system. The AR and DA results can be used to evaluate the acceleration reduction effect and displacement amplification of the QZS system. The data is recorded after the response of the system is stable.

The discrete AR results are plotted in Fig. 17 with the corresponding absolute transmissibility curves (transfer functions) obtained via frequency sweeping tests. The results indicate that the discrete points are consistent

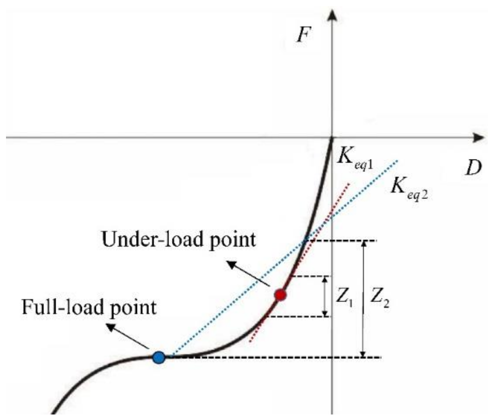

Fig. 16 Change rule illustration of equivalent dynamic stiffness of QZS system

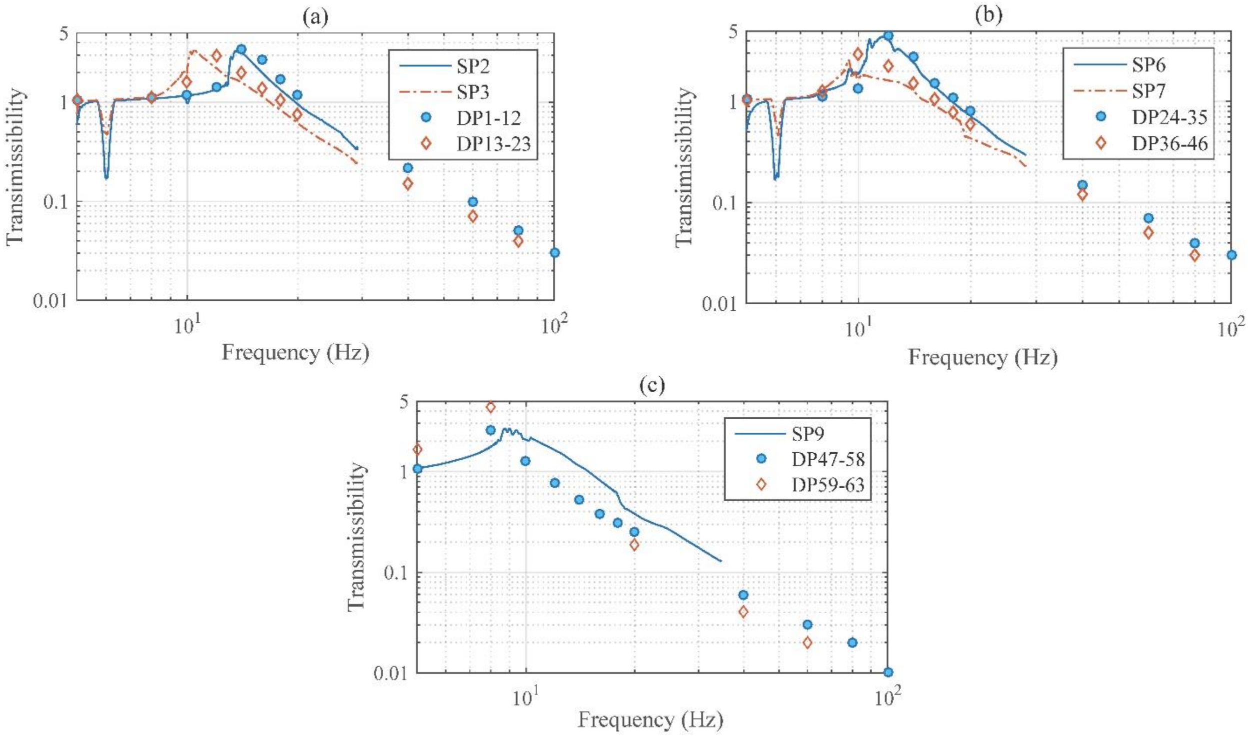

Fig. 17 AR results and absolute transmissibility of (a) isolator A; (b) isolator B; and (c) isolator C

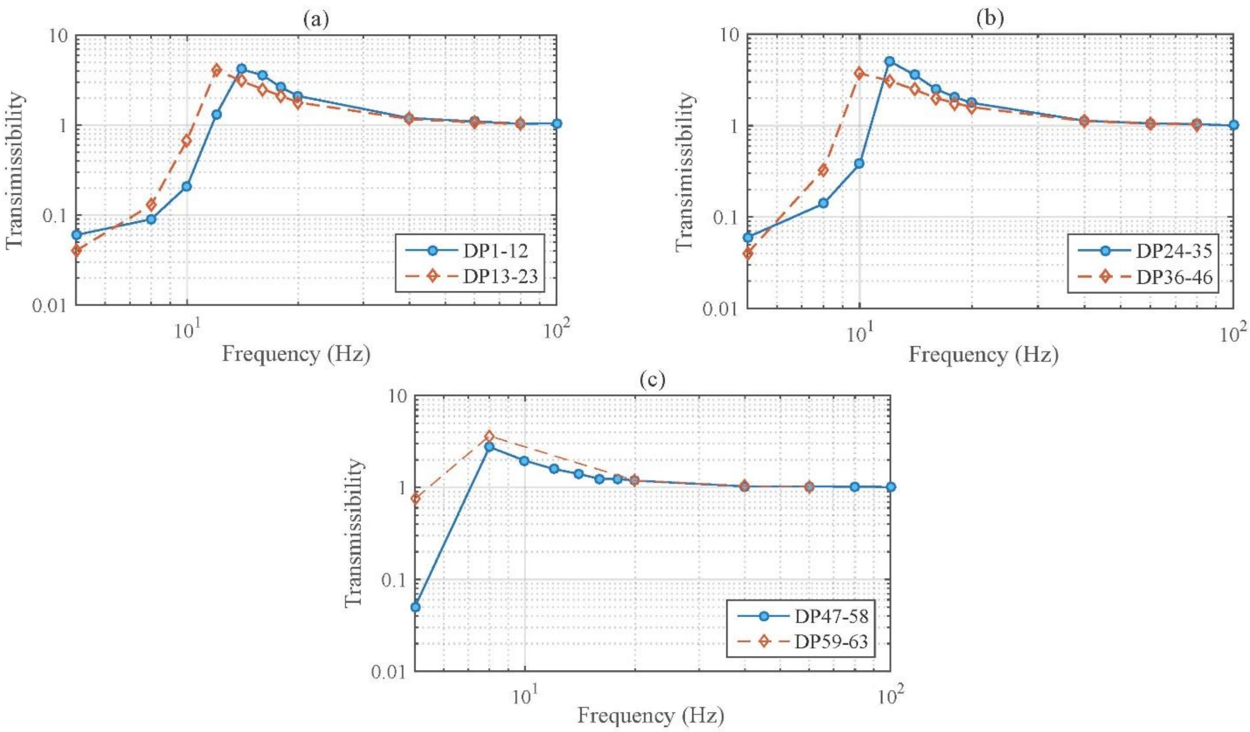

Fig. 18 DA results of (a) isolator A; (b) isolator B; and (c) isolator C

with the transmissibility curves. The two types of results verify each other. The change rule of dynamic properties can also be concluded by the discrete harmonic vibration tests. For the acceleration reduction effect of the system, the high-frequency input components are well mitigated, but there is also an acceleration amplification effect in the resonant region. Another conclusion is that for the high-frequency range after the resonant peak, the AR becomes smaller with the increase in input magnitude, which is the opposite of the low-frequency range before the resonant peak.

The discrete DA results are presented in Fig. 18. The

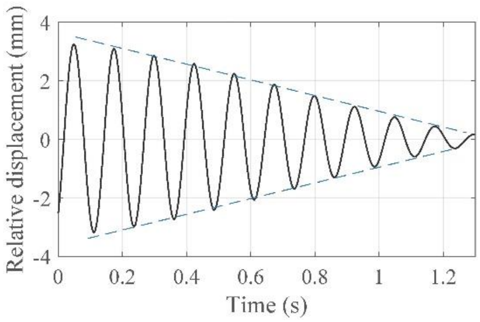

Fig. 19 The free vibration response of DP12

characters of the distribution of DA results are similar to the AR results. Thus, the displacement amplification effect is significant in the resonant region but the absolute displacement input at the shake table is almost absorbed by the isolator in the high-frequency range, and almost no relative displacement occurs at the low-frequency range.

The damping behavior of the QZS system is discussed based on the harmonic vibration tests. The free vibration amplitude decay envelope for the linear viscous and friction type damping can be derived by the slow varying parameter method (Tomlinson and Worden 2000)

$$Y_1(t) = Y_0 e^{-\xi \omega_n t} sin(\omega_n t + \phi_0) \tag{8}$$

$$Y_2(t) = Y_0 - \frac{2c_F}{\pi \omega_n} t \tag{9}$$

where $Y_1(t)$ and $Y_2(t)$ are the decay time history of viscous and friction type damping, Y_0 is the initial displacement, ω_n is the natural frequency, ξ is the linear viscous damping ratio, c_F is the Coulomb friction force, and ϕ_0 is the phase angle.

According to the Eqs. (8) and (9), the decay envelop is linear for friction type damping but logarithmic for the viscous type. Several free vibration results of different cases are shown in Fig. 19. The damping in the QZS system is proved to belong to the friction type. The friction force may exist at the contact surface between the loading setups and disk spring.

Despite the identification of damping type as frictional, the use of an equivalent linear viscous damping ratio to evaluate the damping level of a dynamic system becomes more simplified for its implementation in engineering. It is also proved by previous studies that under the same

Table 6 Impact tests results

Isolator type	Test number	Duration	Design input amplitude	AR	DA
Isolator A	CJ1	10 ms	10 m/s2	0.40	2.06
	CJ2	10 ms	50 m/s2	0.46	2.70
Isolator B	CJ3	10 ms	10 m/s2	0.43	2.13
	CJ4	10 ms	50 m/s2	0.41	2.34
Isolator C	CJ5	10 ms	10 m/s2	0.20	1.97
	CJ6	10 ms	50 m/s2	0.37	3.19

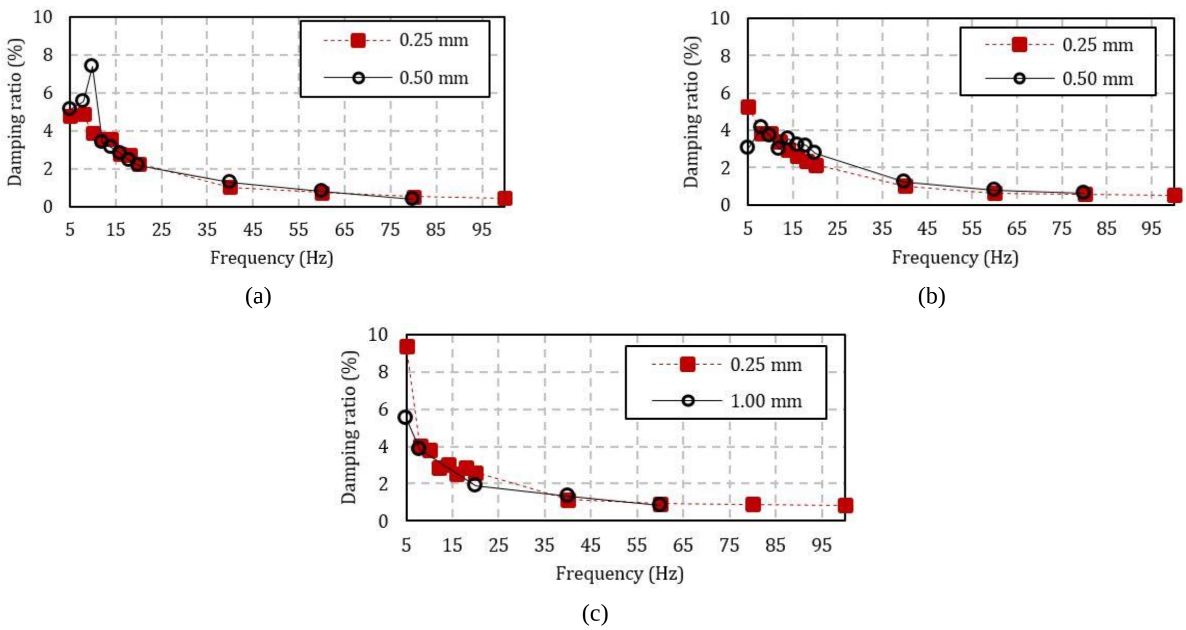

Fig. 20 Equivalent linear viscous damping ratio under different vibration frequencies and input displacement amplitudes of (a) isolator A; (b) isolator B; and (c) isolator C

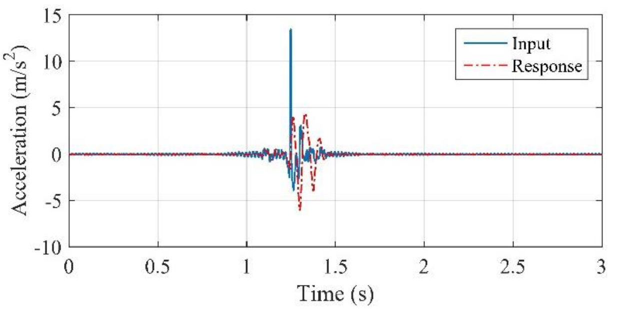

(a)

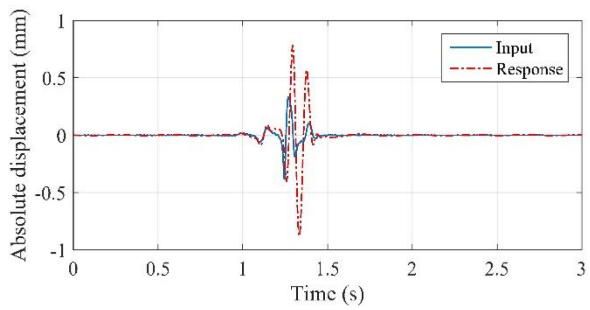

(b)

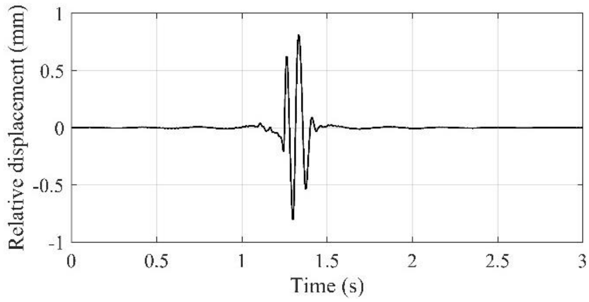

(c)

Fig. 21 Time history response of isolator B under CJ3 impact tests: (a) acceleration response; (b) absolute displacement; and (c) relative displacement

damping level, the dynamic response of frictional and viscous damped systems is similar (Chopra 1995).

Owing to the above consideration, the equivalent linear viscous damping ratios are identified for each harmonic test and listed in Table 6. Fig. 20 presents the equivalent damping ratios for all test cases with input frequency in the horizontal axis. It is concluded that the damping ratio is strongly velocity-depended and it significantly decreases with the increase in loading frequency.

3.4 Impact tests

The impact tests are performed using half-sine input to check the isolation response of the QZS system for impact vibrations. The information on the impact tests and the corresponding main results are listed in Table 6. Typical time history response of impact tests (isolator B) are shown in Fig. 21. Based on the test results, the isolation system can reduce more than half the acceleration response by sacrificing twice the displacement amplification considering the impact of the chosen magnitude.

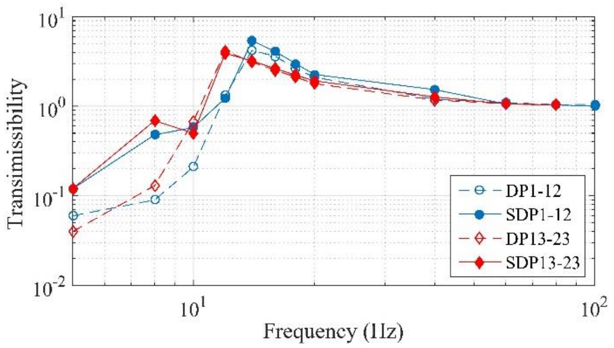

Fig. 22 Transmissibility comparison between numerical and test results

4. Numerical simulation

The QZS isolation system is characterized by its strong stiffness nonlinearity. Generally, the implementation of a linear or equivalent linear calculation approach is difficult to obtain satisfactory simulation results. To evaluate the dynamic response of the system, a user-developed element is created in the OpenSees software that can precisely depict the force-displacement curves of the QZS system. The harmonic vibration tests (DP1-23) and impact tests (CJ1, CJ2) of isolator A are simulated to verify the accuracy of the proposed element and the corresponding simulation method.

Fig. 22 presents the DA result comparison between the numerical and test results. The numerical case SDP1-23 corresponds to the experiment case DP1-23. The test and numerical results consistently correlate in the resonant and high-frequency input regions, and the natural frequency of the nonlinear system can be accurately predicted using the numerical modeling method with the proposed element.

For the impact simulation, the time history response of isolator A under half-sine input is shown in Fig. 23. The typical simulation results are different from the test time history response in Fig. 21, which is due to the shake table input. The control system of the shake table is hard to perform a strictly perfect half-sine input. The comparison of the impact results is listed in Table 7. Except in the test situations, more input amplitudes are selected for simulations. Fig. 24 shows the comparison between AR

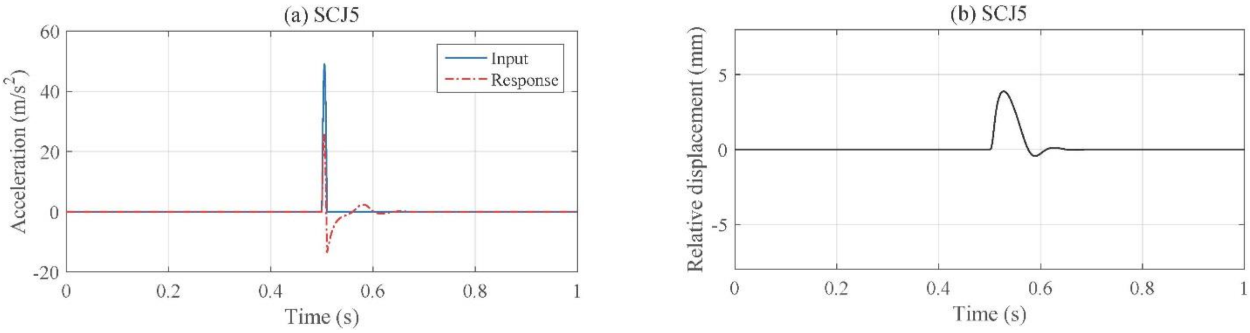

(a) (b)

Fig. 23 Typical simulation time history response of isolator A under impact: (a) absolute acceleration of SCJ5; and (b) relative displacement of SCJ5

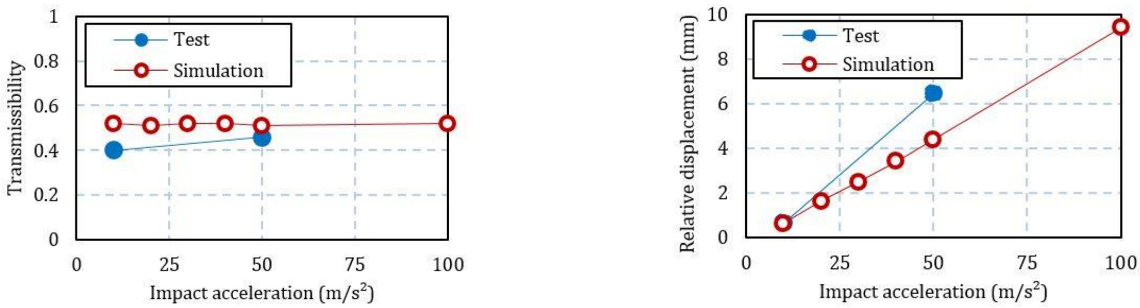

(a) (b)

Fig. 24 Comparison of impact results of isolator A, (a) AR (transmissibility); and (b) relative displacement

Table 7 Comparison between test and simulation impact result (isolator A)

Test number	Simulation number	Input amplitude	AR		Relative displacement (mm)	
			Test	Simulation	Test	Simulation
CJ1	SCJ1	10 m/s2	0.40	0.52	0.64	0.63
--	SCJ2	20 m/s2	--	0.51	--	1.32
--	SCJ3	30 m/s2	--	0.52	--	2.08
--	SCJ4	40 m/s2	--	0.52	--	2.91
CJ2	SCJ5	50 m/s2	0.46	0.51	6.47	3.88
--	SCJ6	100 m/s2	--	0.52	--	9.42

(transmissibility) and relative displacement results. Thus, for the impact response, the corresponding simulations are closer to the test results despite the control issues. The simulations also indicate that even though the transmissibility values remain stable under different peaks of impact, the relative displacement linearly increases with the increase in impact amplitude. More considerations should be addressed on this phenomenon to avoid displacement failure when designing a QZS isolated system subjected to impact.

5. Conclusions

This study introduced a QZS isolation system for vertical isolation. Static tests were performed to verify the force-displacement design and shake table vibration tests were conducted to investigate the dynamic behavior of the QZS system. The numerical simulation method was verified via test and simulation comparison. The main conclusions are summarized below:

- The static tests verify the theoretical force-displacement relation of the proposed QZS system and the two design parameters C and r affect the error values in the test and theoretical results.
- The damping type is identified as frictional. Additional damping is preferred to promote the isolation effect and restrain large isolation displacement. The equivalent damping level decreases when the loading frequency increases.
- The variation law of transmissibility is clear and consistently correlates with the theories:
- For the same input amplitude, the natural frequency

decreases with a decreasing degree of under-load. For the under-load QZS system, the natural frequency increases with increasing input amplitude.

- The transmissibility curves obtained from frequency sweeping tests and harmonic tests consistently correlate and the two results verify each other.
- The isolation effect for the QZS system is adequate for vibrations with frequencies higher than 20 Hz and the amplification effect in the resonant region cannot be neglected.
- The developed element accurately simulates the dynamic response of the QZS system under harmonic and impact vibrations. The transmissibility curves can also be calculated by the time history simulations.

Acknowledgments

The authors acknowledge the financial support from National Natural Science Foundation of China (Grant No. 51878502).

References

Alabuzhev, P., Gritchin, A. and Kim, L. (1989), *Vibration Protecting and Measuring Systems with Quasi-zero Stiffness*, Taylor & Francis Group, New York, NY, USA.

Blair, D.J., Liu, J., Moghaddam, E.F. and Ju, L. (1994), "Performance of an ultra low-frequency folded pendulum", *Phys. Lett. A*, **193**(3), 223-226. https://doi.org/10.1016/0375-9601(94)90587-8

Budiansky, B. (1974), *Theory of Buckling and Post-bucking Behavior of Elastic Structures*, Elsevier, New York, NY, USA.

Carrella, A., Brennan, M.J., Kovacic, I. and Waters, T.P. (2009), "On the force transmissibility of avibration isolator with quasi-zero-stiffness", *J. Sound Vibr.*, **322**(4-5), 707-717. https://doi.org/10.1016/j.jsv.2008.11.034

Chen, L., Sun, L. and Nagarajaiah, S. (2015), "Cable with discrete negative stiffness device and viscous damper: Passive realization and general characteristics", *Smart. Struct. Syst., Int. J.*, **15**(3), 627-643. http://dx.doi.org/10.12989/sss.2015.15.3.627

Chopra, A.K. (1995), *Dynamics of Structures: Theory and Applications to Earthquake Engineering*, Prentice Hall, Englewood Cliffs, NJ, USA.

Cimellaro, G.P., Domaneschi, M. and Warn, G. (2018), "Three-dimensional base isolation using vertical negative stiffness devices", *J. Earthqu. Eng.*, 1-29. https://doi.org/10.1080/13632469.2018.1493004

Demetriades, G.F., Constantinou, M.C. and Reinhorn, A.M. (1993), "Study of wire rope systems for seismic protection of equipment in buildings", *Eng. Struct.*, **15**(5), 321-334. https://doi.org/10.1016/0141-0296(93)90036-4

Farsangi, E.N., Tasnimi, A.A., Yang, T.Y., Takewaki, I. and Mohammadhasani, M. (2018), "Seismic performance of a resilient low-damage base isolation system under combined vertical and horizontal excitations", *Smart. Struct. Syst., Int. J.*, **22**(4), 383-397. http://dx.doi.org/10.12989/sss.2018.22.4.383

Gazi, H. and Alhan, C. (2018), "Probabilistic sensitivity of base-isolated buildings to uncertainties", *Smart. Struct. Syst., Int. J..*, **22**(4), 441-457. http://dx.doi.org/10.12989/sss.2018.22.4.441

Goodwin, A.J.H. (1965), Vibration Isolators; U.S. Patent No. 3,202,388.

Guzman Pujols, J.C. and Ryan, K.L. (2018), "Computational simulation of slab vibration and horizontal-vertical coupling in a full scale test bed subjected to 3D shaking at E-Defense", *Earthq. Eng. Struct. Dyn.*, **47**(2), 438-459. https://doi.org/10.1002/eqe.2973

Halwes, D.R. and Simmons, W.A. (1980), U.S. Patent No. 4, 236,607.

Hu, K., Zhou, Y., Jiang, L., Chen, P. and Qu, G. (2017), "A mechanical tension-resistant device for lead rubber bearings", *Eng. Struct.*, **152**, 238-250. https://doi.org/10.1016/j.engstruct.2017.09.006

Kwon, I.Y., Yang, H.T., Hansma, P.K. and Randall, C.J. (2015), "Implementable bio-inspired passive negative spring actuator for full-scale structural control under seismic excitation", *J. Struct. Eng.*, **142**(1), 04015079. https://doi.org/10.1061/(ASCE)ST.1943-541X.0001323

Lin, T.K., Lu, L.Y. and Chen, C.J. (2018), "Semi-active leverage-type isolation system considering minimum structural energy", *Smart. Struct. Syst., Int. J.*, **21**(3), 373-387. https://doi.org/10.12989/sss.2018.21.3.373

Loh, C.H. and Chao, C.H. (1996), "Effectiveness of active tuned mass damper and seismic isolation on vibration control of multi-storey building", *J. Sound Vibr.* **193**(4), 773-192. https://doi.org/10.1006/jsvi.1996.0315

Lu, L., Duan, Y.F., Spencer, Jr. B.F., Lu, X.L. and Zhou, Y. (2017), "Inertial mass damper for mitigating cable vibration", *Struct. Control. Health Monit.*, **24**(10), e1986. https://doi.org/10.1002/stc.1986

Meng, L., Sun, J. and Wu, W. (2015), "Theoretical design and characteristics analysis of a quasi-zero stiffness isolator using a disk spring as negative stiffness element", *Shock Vib.*, 1-19. http://dx.doi.org/10.1155/2015/813763

Pasala, D.T.R., Sarlis, A.A, Reinhorn, A.M., Nagarajaiah, S., Constantinou, M.C. and Taylor, D. (2014), "Apparent weaken in SDOF yielding structures using a negative stiffness device: Experimental and analytical study", *J. Struct. Eng.*, **141**(4), 04014130. https://doi.org/10.1061/(ASCE)ST.1943-541X.0001077

Platus, D.L. (1992), "Negative-stiffness-mechanism vibration isolation system", In: *Vibration Control in Microelectronics, Optics, and Metrology*, Denver, CO, USA.

Rita, A.D., McGarvey, J.H. and Jones, R. (1978), "Helicopter rotor isolation evaluation utilizing the dynamic antiresonant vibration isolator", *J. Am. Helicopter Soc*., **23**(1), 22-29. https://doi.org/10.4050/JAHS.23.22

Rivin, E.I. (2003), *Dynamic Properties of Vibration Isolation Systems*, Asme Press, New York, NY, USA.

Sarlis, A.A., Pasala, D.T.R., Constantinou, M.C., Reinhorn, A.M., Nagarajaiah, S. and Taylor, D. (2012), "Negative stiffness device for seismic protection of structures", *J. Struct. Eng.*, **139**(7), 1124-1133. https://doi.org/10.1061/(ASCE)ST.1943-541X.0000616

Sciulli, D. and Inman, D.J. (1998), "Isolation design for a flexible system", *J. Sound Vib.*, **216**(2), 251-267. https://doi.org/10.1006/jsvi.1998.1667

Shi, X. and Zhu, S.Y. (2015), "Magnetic negative stiffness dampers", *Smart Mater. Struct.*, **24**(7), 072002. https://doi.org/10.1088/0964-1726/24/7/072002

Shi, X. and Zhu, S.Y. (2017), "Simulation and optimization of magnetic negative stiffness dampers", *Sens. Actuator A-Phys.*, **259**, 14-33. https://doi.org/10.1016/j.sna.2017.03.026

Shi, X., Zhu, S.Y., Ni, Y.Q. and Li, J. (2018), "Vibration suppression in high-speed trains with negative stiffness dampers", *Smart. Struct. Syst., Int. J.*, **21**(5), 653-668. https://doi.org/10.12989/sss.2018.21.5.653

Tomlinson, G.R. and Worden, K. (2000), *Nonlinearity in Structural Dynamics: Detection, Identification and Modelling*, CRC Press, Boca Raton, FL, USA.

Walsh, K.K., Boso, E., Steinberg, E.P., Haftman, J.T. and Littell, W.N. (2018), “Variable negative stiffness device for seismic protection of building structures through apparent weakening”, *J. Eng. Mech.*, **144**(9), 04018090. https://doi.org/10.1061/(ASCE)EM.1943-7889.0001512

Winterflood, J. and Blair, D.G. (1998), “A long-period vertical vibration isolator for gravitational wave detection”, *Phys. Lett. A*, **243**(1-2), 1-6. https://doi.org/10.1016/S0375-9601(98)00193-5

Winterflood, J., Losurdo, G. and Blair, D.G. (1999), “Initial results from a long-period conical pendulum vibration isolator with application for gravitational wave detection”, *Phys. Lett. A*, **263**(1-2), 9-14. https://doi.org/10.1016/S0375-9601(99)00715-X

Zheng, Y., Li, Q., Yan, B., Luo, Y. and Zhang, X. (2018), “A stewart isolator with high-static-low-dynamic stiffness struts based on negative stiffness magnetic springs”, *J. Sound Vibr.* **422**, 390-408. https://doi.org/10.1016/j.jsv.2018.02.046

Zhou, Y. and Chen, P. (2017), “Shaking table tests and numerical studies on the effect of viscous dampers on an isolated RC building by friction pendulum bearings”, *Soil Dyn. Earthq. Eng.*, **100**, 330-344. https://doi.org/10.1016/j.soildyn.2017.06.002

Zhou, Y., Chen, P. and Mosqueda, G. (2019), “Analytical and numerical investigation of quasi-zero stiffness vertical isolation system”, *J. Eng. Mech.*, **145**(6), 04019035. https://doi.org/10.1061/(ASCE)EM.1943-7889.0001611.

BS